Optical Engineering

OpticalEngineering.SPIEDigitalLibrary.org

Substructured Ronchi gratings from the linear combination of classical gratings

Daniel Aguirre-Aguirre
Brenda Villalobos-Mendoza
Fermín S. Granados-Agustín
Rafael Izazaga-Pérez
Manuel Campos-García
María Elizabeth Percino-Zacarías
Alejandro Cornejo-Rodríguez

SPIE.

Substructured Ronchi gratings from the linear combination of classical gratings

Daniel Aguirre-Aguirre,[a,*] Brenda Villalobos-Mendoza,[a] Fermín S. Granados-Agustín,[a] Rafael Izazaga-Pérez,[a] Manuel Campos-García,[b] María Elizabeth Percino-Zacarías,[a] and Alejandro Cornejo-Rodríguez[a]
[a]Instituto Nacional de Astrofísica, Óptica y Electrónica, Departamento de Óptica, INAOE, Apdo. Postal 51 and 216, C. P. 72000, Puebla, México
[b]Universidad Nacional Autónoma de México, Centro de Ciencias Aplicadas y Desarrollo Tecnológico, Apdo. Postal 70-186, 04510 D. F. México, México

Abstract. Substructured Ronchi gratings are used to sharpen and increase the number of fringes in Ronchigrams, thereby increasing their spatial resolution and allowing greater accuracy in the evaluation of a surface under test. This work presents a simple method for generating substructured Ronchi gratings and for calculating the intensity pattern produced by this type of grating. For this, we propose the generation of this kind of grating from the linear combination of classical gratings; the pattern of irradiance produced by these Ronchi gratings will be a linear combination of the intensity patterns produced by each combined classical grating. A comparison between theoretical and experimental Ronchigrams was obtained by analyzing a parabolic mirror. [DOI: 10.1117/1.OE.53.11.114111]

Keywords: Ronchi test; optical testing; optical systems.

Paper 141120 received Jul. 13, 2014; accepted for publication Oct. 24, 2014; published online Nov. 21, 2014.

1 Introduction

The Ronchi test is one simple and powerful method used in optical workshops for measuring deformations in concave surfaces and optical systems in general, since the errors of the surface can be estimated by the deviation of the fringe pattern observed at the exit pupil when it is compared with the calculated theoretical pattern.[1–5] The test setup consists of illuminating with an extended light source the half of the Ronchi grating placed near the paraxial radius of the curvature of the surface under test, and observing the image produced with the other half of the grating; this produces an interference pattern that can be observed at the exit pupil of the surface of the optical system under test[2,4,6–8] (Fig. 1).

The fringes in the Ronchi test are usually studied using geometrical theory,[9] in which Ronchigram fringes are the result of rays deviating from their ideal path, which is caused by the errors in the slopes of the surface under test [Fig. 2(a)]. On the other hand, with wave theory, the fringes are caused by interference between the overlapping of the diffracted wavefronts[10] [Fig. 2(b)]. Therefore, this test can be seen as a lateral displacement interferometer that measures the slopes of the wavefront instead of measuring the wavefront as in conventional interferometry.[1,2]

2 Substructured Gratings

The substructured gratings were proposed by Murty and A. Cornejo[11] with the aim of sharpening the fringes observed in the interference pattern when using the Ronchi test; other works about the substructured Ronchi gratings were analyzed in Refs. 12–15, mainly using Katyl's ruling proposal.[16] An unequal configuration of the width of transparent and opaque bands on the grating is used for these substructured rulings; if the transparent bands are wider than the opaque ones, the purposed grating is considered positive, and if the opaque fringes are wider than the transparent ones, it is considered negative.[12,13,17]

Ronchi substructured gratings have the same period as conventional gratings; in other words, substructured gratings are based on classical gratings, but unlike these, each opaque and transparent band features an internal substructure Fig. 3.

This paper proposes the use of substructured gratings with different sequences, but constructed with the overlapping of classical Ronchi gratings; the main purpose is increasing the contrast of the interference compared with classical Ronchi rulings.

3 Substructured Gratings Theory

Considering the typical geometry used in the Ronchi test for analyzing converging wave fronts (Fig. 1), the transmittance of a classical Ronchi grating can be expressed in the following manner:[18]

$$M(x_r) = 1 + \cos\left(\frac{2\pi x_r}{d} - \beta\right) \begin{cases} 0 & \text{if } M(x_r) \le 1 \\ 1 & \text{if } M(x_r) > 1 \end{cases}, \tag{1}$$

where d is the grating period, and β is a lateral displacement parameter determined by the initial position of the grating.[4–6,19]

Once the grating is placed in the plane where the aberrated wavefront will be measured, a distorted irradiance pattern will be obtained due to the aberrations of the wavefront coming from the surface under test; this intensity pattern can be expressed as

*Address all correspondence to: Daniel Aguirre-Aguirre, E-mail: daguirreaguirre@gmail.com

0091-3286/2014/$25.00

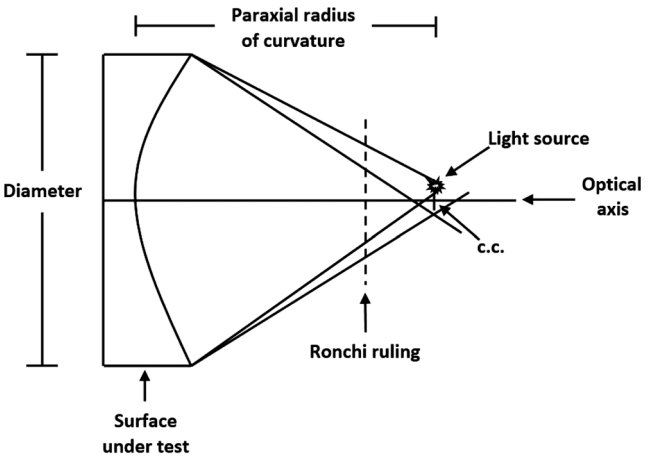

Fig. 1 Configuration of the Ronchi test.

$$I(x,y) = a(x,y) + b(x,y)\cos\left(\frac{2\pi\,\mathrm{OPD}}{\lambda} - \beta\right), \tag{2}$$

where $a(x,y)$ and $b(x,y)$ are the background and local contrast coefficients, respectively, while the optical path difference (OPD) in the lateral displacement interferometer is determined by the difference between the original wavefront and the shifted wavefront,[2,4,5,19–21]

$$\mathrm{OPD} = \frac{\partial W(x,y)}{\partial x}\Delta x = W(x,y) - W(x+\Delta x, y);$$
$$\mathrm{OPD} = \frac{\partial W(x,y)}{\partial y}\Delta y = W(x,y) - W(x,y+\Delta y); \tag{3}$$

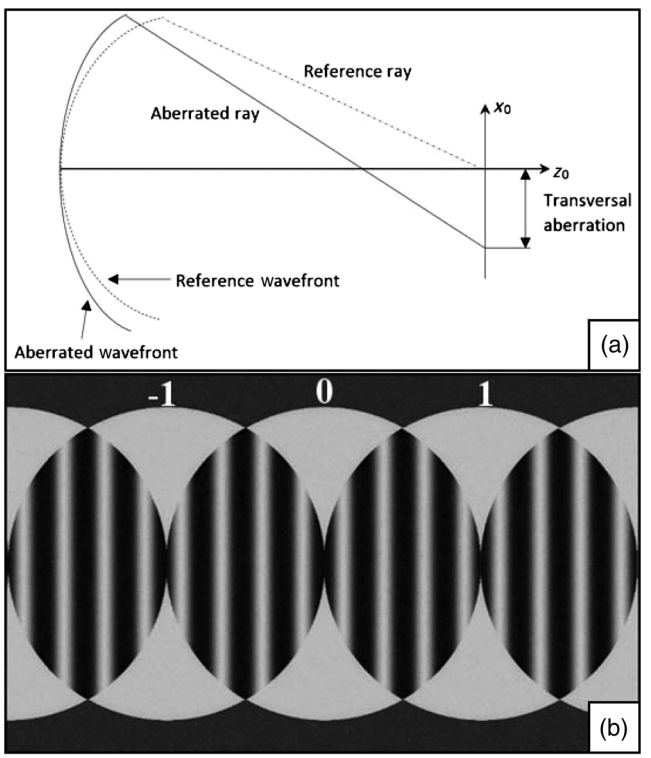

Fig. 2 Ronchi test from the point of view of (a) geometric theory and (b) wave theory.

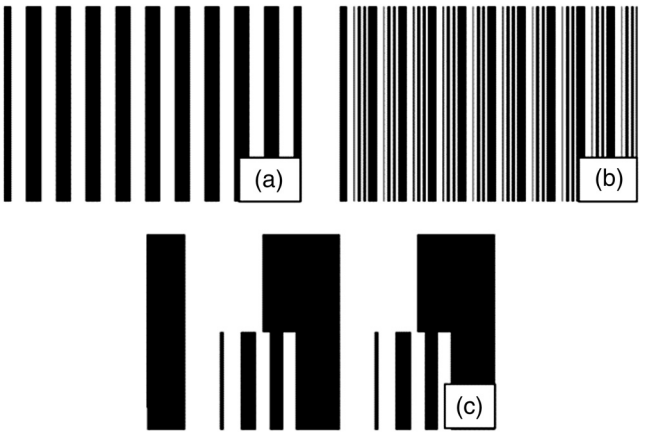

Fig. 3 Ronchi gratings; (a) classical, (b) substructured (c) comparison of the two gratings (a) and (b).

where Δx and Δy are the lateral displacements in both the x and y axes; $W(x+\Delta x, y)$ and $W(x, y+\Delta y)$ represent the wavefront shifted along the x and y axes, respectively, while $W(x,y)$ represents the original wavefront.

On the other hand, considering the differences between the sagittae of the conical surface to be tested $[z(x,y)]$ and an osculatory sphere $[z_o(x,y)]$,[2,20,21] we have

$$2W(x,y) = z(x,y) - z_o(x,y). \tag{4}$$

Assuming that the grating lines are parallel to the y axis, the substructured Ronchi grating can be expressed, in general, as the linear combination of classical gratings with different frequencies,[15] therefore

$$M(x_r) = \sum_{m=1}^{n} 1 + \cos\left(\frac{\delta_m \pi x_r}{2d} - \beta_m\right)$$
$$= \sum_{m=1}^{n} 1 + \cos\left(\frac{2\pi x_r}{d_m} - \beta_m\right)\begin{cases} 0 & \text{if } M(x_r) \le n \\ 1 & \text{if } M(x_r) > n \end{cases}, \tag{5}$$

where δ can take a value of $1, 2, 3, 4, \ldots, \infty$.

Considering that substructured Ronchi gratings are formed from the linear combination of classical gratings of different frequencies, it is intuitive to think that the intensity pattern observed at the exit pupil with this type of grating will also be a linear combination of the interference intensity patterns produced by each classical grating; therefore, the intensity function at the exit pupil of a system for a substructured grating will be given by

$$I(x,y) = \sum_{m=1}^{n} a(x,y) + b(x,y)\cos\left(\frac{m\pi\,\mathrm{OPD}}{2\lambda} - \beta_m\right). \tag{6}$$

Figure 4 shows the two different methods presented in this work to generate substructured Ronchigrams. The first way is to generate a substructured grating overlapping two classical rulings, from Figs. 4(a) to 4(b); introduce the grating of Fig. 4(b) in the experimental Ronchi's setup and the Ronchigram of Fig. 4(d) is registered. This last Ronchigram is equivalent if two experimental Ronchigrams of Fig. 4(c)

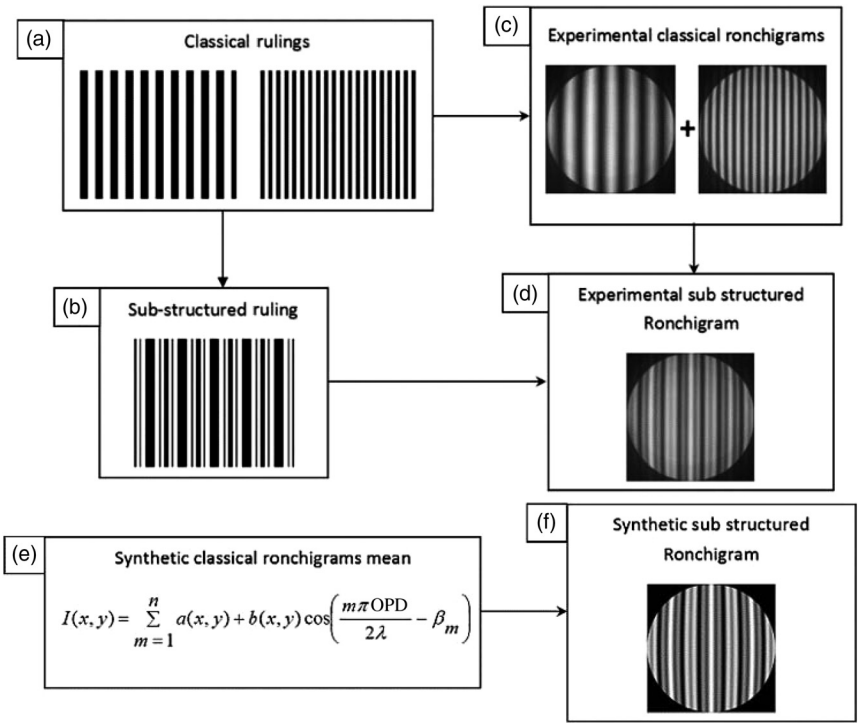

Fig. 4 Flowchart representing the different ways for obtaining a substructured Ronchigram, (a) to (d) refer to the combination of classical gratings; (e) and (f) refer to a synthetic ruling.

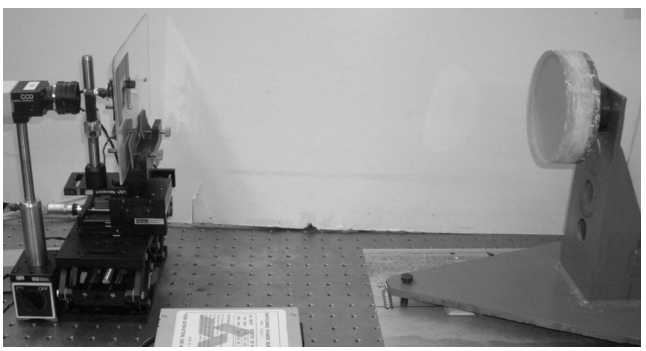

Fig. 5 Experimental setup.

are added. In Figs. 4(e) and 4(f), using Eqs. (5) and (6), a synthetic Ronchigram is obtained starting with the classical gratings of Fig. 4(a).

For comparison of the simulated Ronchigram with the experimental Ronchigram under the criterion of two-dimensional correlation between two images,[22] we generate an algorithm for the calculation of the correlation within the exit pupil of the system, with the equation

$$C=\frac{\sum_m \sum_n (A_{mn}-\bar{A})(B_{mn}-\bar{B})}{\sqrt{(\sum_m \sum_n (A_{mn}-\bar{A})^2)(\sum_m \sum_n (B_{mn}-\bar{B})^2)}}, \tag{7}$$

Characteristic	Synthetic Ronchigrams	Experimental Ronchigrams
$m=2$ $\delta_1=2;\delta_2=5$ $\beta_1=\beta_2=0$	(a)	(b)
$m=2$ $\delta_1=4;\delta_2=5$ $\beta_1=\beta_2=0$	(c)	(d)

Fig. 6 Ronchigrams obtained with substructured grating generated with $m=2$, Eq. (5).

Characteristic	Synthetic Ronchigrams	Experimental Ronchigrams
$m=3$ $\delta_1=3;\delta_2=5;\delta_3=6$ $\beta_1=\beta_2=\beta_3=0$	(a)	(b)
$m=3$ $\delta_1=4;\delta_2=1;\delta_3=6$ $\beta_1=\beta_2=\beta_3=0$	(c)	(d)

Fig. 7 Ronchigrams obtained with substructured grating generated with $m=3$, Eq. (5).

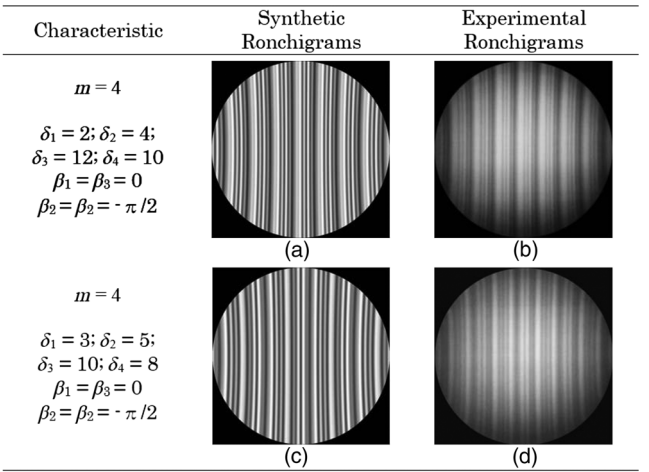

Fig. 8 Ronchigrams obtained with substructured grating generated with $m = 4$, Eq. (5).

where A and B are the matrices of the intensity values of the simulated and experimental Ronchigrams, respectively; while $\bar{A}$ and $\bar{B}$ are the average intensity levels of their respective Ronchigrams.[22] C takes values between 0 and 1, where 0 means that they are not equal and 1 means that the images are equal.

4 Experimental Results

For this section, we used a spatial light modulator (SLM) to create the light and dark bands of the Ronchi ruling due to the various advantages provided by this kind of device.[13,15,23–26] The substructured Ronchi gratings are deployed in the SLM with a spatial resolution of 1024×768 pixels, giving an active area of 26.6×19.9 mm^2. The SLM is on a mount capable of micrometric movements on both x and y axes; these movements provide defocus and changes in the β coefficient, respectively. The light source is a light emitting diode with a predominant wavelength of 700 nm.

A parabolic concave mirror was tested with a curvature radius of 397.55 mm and a diameter of 57.27 mm. The period of the Ronchi gratings used in this analysis was 0.847 mm (equivalent to 30 lpi in a classical grating). Figure 5 is the experimental set up used for this Ronchi test.

The images in Fig. 6 were obtained by placing the SLM at a distance of 370.55 mm from the apex of the surface under test. This position of the grating is often called intrafocal, as the grating moves toward the mirror. The number of classical gratings used for generating a substructured grating was two with different periods, and the gap between them was zero.

It can be seen that the experimental Ronchigrams are qualitatively similar to the synthetic Ronchigrams obtained with Eq. (6), showing a correlation value >0.8, by using Eq. (7).

The images shown in Figs. 7 and 8 were obtained at a distance of 370.55 mm from the apex of the mirror under test. This position of the grating is often called extrafocal, since the grating moves away from the mirror. The Ronchigrams images shown in these figures were generated with substructured gratings, which are obtained by the combination of three and four classical gratings with different periods.

Figure 9(a) shows a cross section on the centerline of the classical (dots) and substructured (line) Ronchigrams; the figure shows the increase of maximum and minimum values, which results in an increase of the spatial resolution of the test.

Furthermore, Fig. 9(b) shows the comparison between the irradiance profiles of the Ronchigrams shown in Figs. 7(c) and 7(d), which differ only in background and local contrast.

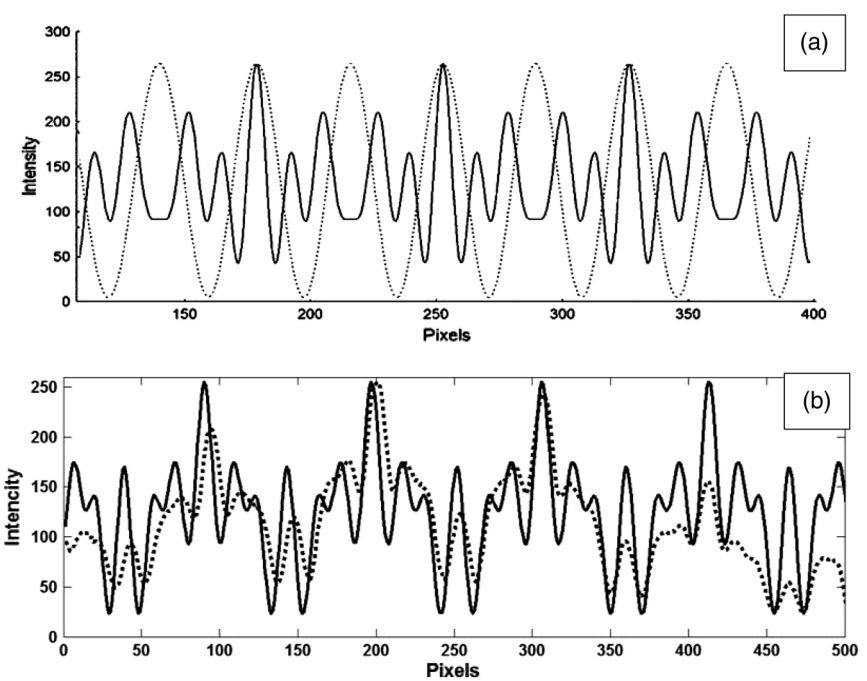

Fig. 9 Intensity pattern of a cross section for (a) a classical Ronchigram (dots) and substructured Ronchigrams shown in Fig. 7(a) (line), and (b) part of the substructured Ronchigrams shown in Figs. 7(c) (dots) and 7(d) (line).

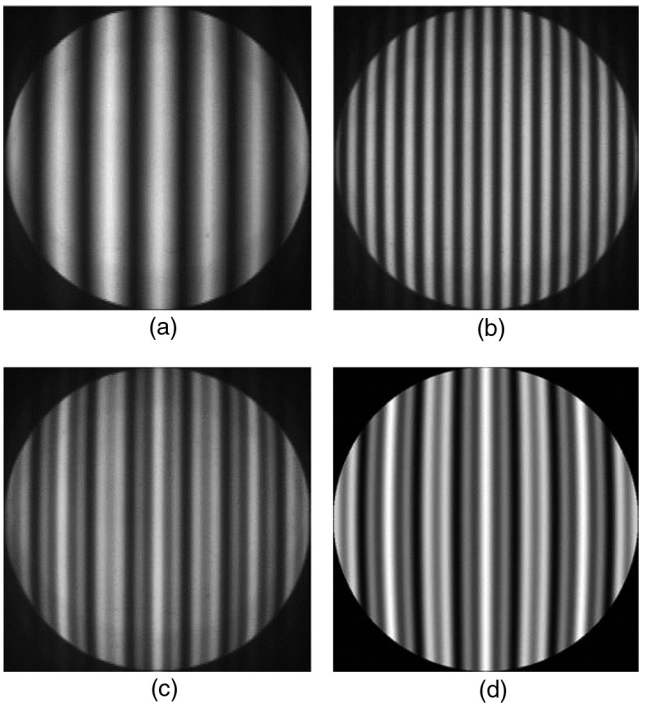

Fig. 10 (a) Classical Ronchigram obtained with 30-lpi grating; (b) classical Ronchigram obtained with 75-lpi grating; (c) sum of images 4(a) and 4(b); (d) calculated theoretical Ronchigram.

This is due to the conditions of the test in the laboratory, which reduced the contrast and/or the homogeneity of lighting of the Ronchigrams.[19]

5 Linear Combination of Classical Ronchigrams

To experimentally verify that the substructured irradiance Ronchigrams patterns can be derived by the linear combination of the classical intensity Ronchigrams patterns produced for its corresponding combined classical gratings, an n number of Ronchigrams with classical gratings of different frequencies were obtained at a distance of 379.55 cm from the apex of the mirror. The linear combination of classical Ronchigrams was done with the average of the sum, pixel by pixel, of the intensity levels of each of the combined images as follows:

$$\text{Ronchigram sub} = \frac{1}{n}\sum_{m=1}^{n}\text{Ronchigram clas}_m. \tag{8}$$

Figure 10(c) shows the linear combination of two Ronchigrams taken with gratings of 30 [Fig. 10(a)] and 75 lines [Fig. 10(b)] per inch, which is identical in form to the Ronchigram theoretically calculated using a substructured grating [Fig. 10(d)].

The Fig. 11(d) shows the linear combination of three classical Ronchigrams taken with gratings of 45 [Fig. 11(a)], 75 [Fig. 11(b)] and 90 lines [Fig. 11(c)] per inch, which is identical in form to the Ronchigram theoretically calculated using a substructured grating [Fig. 11(e)], with a correlation value >0.9. The difference of intensity between the images of Figs. 11(d) and 11(e) is due to lighting problems in the laboratory when the experimental Ronchigrams were taken.

6 Synthetic Ronchigrams for Primary Aberrations

Denoting $W(x,y)$ as the aberration polynomial given by Kingslake[27] for primary aberrations, we could calculate the irradiance pattern produced by a surface with this type of aberration in the following form:

$$W(x,y) = A(x^2+y^2)^2 + By(x^2+y^2) + C(x^2+3y^2) + D(x^2+y^2), \tag{9}$$

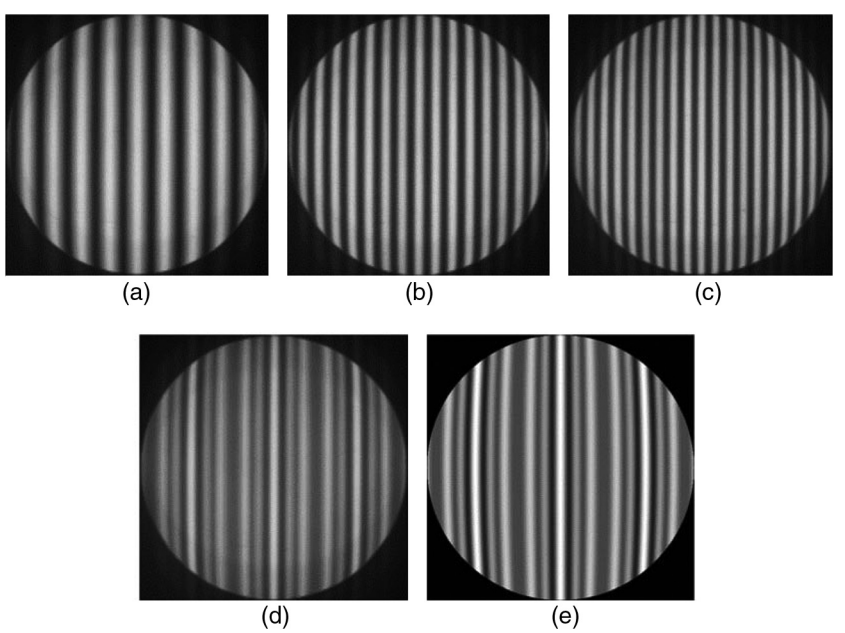

Fig. 11 (a) Classical Ronchigram obtained with 45-lpi grating; (b) classical Ronchigram obtained with 75-lpi grating; (c) classical Ronchigram obtained with 90-lpi grating; (d) sum of images 5(a), 5(b) and 5(c); (e) calculated theoretical Ronchigram.

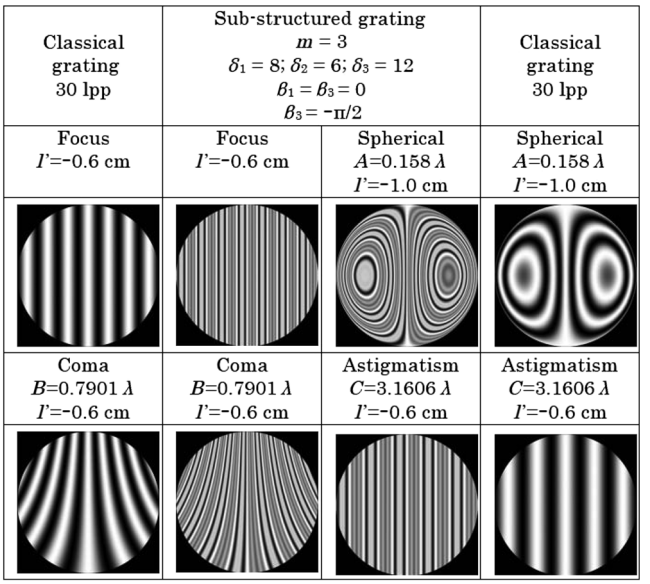

Fig. 12 Synthetic Ronchigrams with different types of primary aberrations obtained with a substructured grating $m = 3$.

where A is the spherical aberration coefficient, B is the coma coefficient, C the astigmatism coefficient, and D is the defocus coefficient, which may remain constant because it depends only on the position of the grating l and on the paraxial radius of curvature r of the surface under test,[2,20,21] which is equal to

$$D = \frac{l}{2r^2}. \tag{10}$$

Thus, the intensity pattern at the exit pupil will be given according to Eq. (6) written as

$$I(x,y) = \sum_{m=1}^{n} a(x,y) + b(x,y)\cos \times \left(\frac{m\pi(W(x,y) - W(x+\Delta x,y))}{2\lambda} - \beta_m\right) \tag{11}$$

with the OPD written as the difference between the original and shifted wavefronts $W(x,y)$ and $W(x+\Delta x,y)$, respectively.

Figure 12 shows in the left side the synthetic Ronchigrams intensity patterns produced using the Ronchi test with a substructured grating with $m = 3$, as well as the intensity patterns produced with a classical grating of 30 lpi for different values of the aberration coefficients.

With a comparison from Fig. 12 between the synthetic and experimental Ronchigrams using substructured and classical Ronchi rulings, the main difference is that the Ronchigrams fringes are sharper when substructure rulings are used.

7 Conclusions

In this work, we present the equations needed to generate, in a simple way, substructured Ronchi gratings and to calculate the irradiance pattern produced with such gratings.

It was demonstrated that the use of substructured gratings is useful for thinning the fringes and increasing the spatial resolution of these gratings, as is evident when comparing classical Ronchi gratings with substructured Ronchi gratings. Using substructured gratings increases the number of fringes that appear in the irradiance pattern compared to classical Ronchi gratings. It is worth noting that this type of grating was used for the analysis of different conical surfaces (parabolic, hyperbolic, and spherical), giving similar results to those presented in Sec. 4.

On the other hand, as an alternative method to produce substructured gratings and its corresponding Ronchigrams, it was shown that if two or more Ronchigrams obtained with classical gratings of different frequencies are combined, it is possible to generate substructured Ronchi patterns identical to those obtained when using substructured gratings. This is important because when an SLM in which the substructured gratings can be deployed is not available, or when there is no method to make substructured gratings in the classical manner (engraving glass, acetate sheets, etc.) and there are only classical gratings of different frequencies, it is possible to use the method of combining two or more different classical Ronchi rulings by using the corresponding Ronchigrams of different frequencies and synthetically generating substructured Ronchigrams.

Then it is possible to use the method of combining two or more classical Ronchi rulings with different frequencies to produce a substructured grating. Similarly, Ronchigrams with substructured gratings can be synthetically generated, overlapping classical Ronchigrams obtained with classical rulings.

Acknowledgments

Villalobos-Mendoza and Izazaga-Perez thank the CONACyT (México) for the scholarships granted, CVU: 272864 and 270587, respectively. We also thanks to Jose Miguel Arroyo Hernandez Technician of INAOE's optical shop, for polishing the surfaces under test.

References

1. V. Ronchi, "Le frange di combinazioni nello studio delle superficie e dei sistemi ottici," *Riv. Ottica Meec. Precis.* **2**(4), 9–35 (1923).
2. A. Cornejo-Rodríguez, "Ronchi Test," in *Optical Shop Testing*, Chap. 9, D. Malacara, Ed., A. John Wiley & Sons, New York (2007).
3. A. Cordero-Dávila, A. Cornejo-Rodríguez, and O. Cardona Nunez, "Ronchi and Hartmann tests with the same mathematical theory," *Appl. Opt.* **31**(13), 2370–2376 (1992).
4. M. Servin, D. Malacara, and F. Cuevas, "Direct-phase detection of modulated Ronchi ruling using a phase-locked loop," *Opt. Eng.* **33**(4), 1193–1199 (1994).
5. K. Hibino et al., "Dynamic range of Ronchi test with a phase-shifted sinusoidal grating," *Appl. Opt.* **36**(25), 6178–6189 (1997).
6. W. S. Meyers and H. P. Stahl, "Sensitivity of two-channel Ronchi test to grating misalignment," *Proc. SPIE* **1994**, 90–101 (1994).
7. W. Der-Shen and C. Ming-Wen, "Effects of grating spacing on the Ronchi test," *Opt. Eng.* **32**(5), 1084–1090 (1993).
8. J. A. Anderson and R. W. Porter, "Ronchi's method of optical testing," *Astrophys. J.* **70**, 175–181 (1929).
9. D. Malacara, "Geometrical Ronchi test of aspherical mirrors," *Appl. Opt.* **4**, 1371–1374 (1965).
10. A. Cornejo and D. Malacara, "Ronchi test of aspherical surfaces, analysis, and accuracy," *Appl. Opt.* **9**(8), 1897–1901 (1897).
11. M. V. R. Murty and A. Cornejo, "Sharpening the fringes in the Ronchi test," *Appl. Opt.* **12**, 2230–2231 (1973).
12. A. Cornejo-Rodríguez, F. Granados-Agustín, and Y. Luna-Zayas, "The Ronchi test and the use of structured gratings for sharpening the fringes," in *Frontiers in Optics, OSA Technical Digest (CD)*, Optical Society of America, paper OFWA1 (2006).
13. D. Aguirre-Aguirre et al., "Evaluation of the increment of the sampling in optical testing using substructured Ronchi gratings," *J. Phys.: Conf. Ser.* **274**(1), 012062 (2011).

14. A. Cornejo, H. Altamirano, and M. V. R. K. Murty, "Experimental results in the sharpening of the fringes in the Ronchi test," *Bol. Inst. Tonantzintla* **2**(4), 313–315 (1978).
15. J. Salinas-Luna et al., "Ronchi test with variable-frequency rulings," *Opt. Eng.* **48**(1), 013604 (2009).
16. R. H. Katyl, "Moiré screens coded with pseudo-random sequences," *Appl. Opt.* **11**, 2278–2285 (1972).
17. M. Campos and F. S. Granados, "Interferometric Ronchi test by using substructured gratings," *Proc. SPIE* **7390**, 73901B (2009).
18. R. Barakat, "General diffraction theory of optical aberration tests, from the point of view of spatial filtering," *J. Opt. Soc. Am.* **59**, 1432–1439 (1969).
19. D. Malacara, M. Servín, and Z. Malacara, *Interferogram Analysis for Optical Testing*, Taylor & Francis Group, New York (2005).
20. D. Aguirre-Aguirre et al., "Obtaining the wavefront in the Ronchi test using only one Ronchigram with random coefficients of aberration," *Opt. Eng.* **52**(5), 053606 (2013).
21. D. Aguirre-Aguirre et al., "Simulation algorithm for Ronchigrams of spherical and aspherical surfaces, with the lateral shear interferometry formalism," *Opt. Rev.* **20**(3), 271–276 (2013).
22. M. R. Spiegel, *Theory and Problems of Probability and Statistics*, 2nd ed., Chap. 14, p. 294, McGraw-Hill, New York (1992).
23. M. Mora-González and N. Alcalá-Ochoa, "The Ronchi test with a LCD grating," *Opt. Commun.* **191**, 203–207 (2001).
24. N. Alcalá-Ochoa, M. Mora González, and F. Mendoza Santoyo, "Flatness measurement by a grazing Ronchi test," *Opt. Express* **11**(18), 2177–2182 (2003).
25. J. Castro-Ramos, S. Vázquez-Montiel, and A. Padilla-Vivanco, "Phase shifting interferometry by using a LCD and bironchi test," *Proc. SPIE* **5622**, 639–645 (2004).
26. M. Mora-González and N. Acalá-Ochoa, "Sinusoidal liquid crystal display grating in the Ronchi test," *Opt. Eng.* **42**(6), 1725–1729 (2003).
27. R. Kingslake, "The interferometer patterns due to the primary aberrations," *Trans. Opt. Soc.* **27**(2), 94–105 (1925).

Daniel Aguirre-Aguirre received his engineering physics degree in 2007 from the Engineering and Technology Institute (IIT-UACJ), Chihuahua, México. He received his MS and PhD degrees in optics in 2010 and 2014, respectively, both from the National Institute of Astrophysics, Optics, and Electronics (INAOE), Puebla, México. His research interests include optical metrology, digital image processing, and instrumentation.

Brenda Villalobos-Mendoza is a member of SPIE, currently a PhD candidate at the National Institute for Astrophysics, Optics and Electronics (INAOE), Puebla, México. She received her engineering degree from the Universidad Autónoma de Ciudad Juárez (UACJ), México, in 2008, and her MS in optics from Benemérita Universidad Autónoma de Puebla (BUAP), Puebla, México, in 2010. She has experience in optical testing in the laboratory and her research interest includes interferometric optical testing and phase shifting interferometry.

Fermín S. Granados-Agustín is a researcher in the Optics Department of the National Institute of Astrophysics, Optics, and Electronics (INAOE), México. He received his BS degree in physics from the National University of México (UNAM), in 1993. He received his MS and PhD degrees in optics, respectively, in 1995 and 1998, both from the INAOE. He is a national researcher for the National System of Researchers, México. He held a postdoctoral position at the mirror lab of the Steward Observatory at the University of Arizona, in 1999. He has been the head of the optical shop at the INAOE since 2005. His research interest included optical information, interferometric optical testing, and instrumentation.

Rafael Izazaga-Pérez received his BS degree in electromechanical engineering from Acapulco Technological Institute (ITA), Guerrero, México, in 2008 and his MS degree in applied physics from Puebla Autonomous University (BUAP), Puebla, México, in 2010. He is a member of SPIE and currently a PhD candidate at the National Institute for Astrophysics, Optics and Electronics (INAOE), Puebla, México. He has experience in optical fabrication and testing at INAOE's optical workshop. His last research interests include stressed mirror polishing, optical metrology, and instrumentation.

Manuel Campos-García is a researcher in the Universidad Nacional Autónoma de México (UNAM). He received his BS, MS, and PhD degrees in physics from UNAM. He held a postdoctoral position at the National Institute for Astrophysics, Optics and Electronics (INAOE), Puebla, México. He is a national researcher for the National System of Researchers, México. His research interest included instrumentation, aspheric surface testing, and optical metrology.

Maria E. Percino-Zacarias got a physics degree from FCFM of BUAP, and MS and PhD degrees in optics from INAOE. Since 2009 she has worked at INAOE's Optical Shop. She supervises the fabrication and optical tests of each optical element that is manufactured there.

Alejandro Cornejo-Rodríguez received his physics degree in 1964 from the Universidad Nacional Autónoma de México, his MS degree in optics in 1968 from Rochester University, and his PhD degree in optics in 1982 from Tokyo Institute of Technology, Japan. He is now a senior researcher in the Optics Department at the National Institute of Astrophysics, Optics, and Electronics (INAOE), México. His research interests include optical metrology, optical surface testing, and optical image processing.